PERGAMON

Scripta mater. 42 (2000) 855–860

Scripta MATERIALIA

www.elsevier.com/locate/scriptamat

THE DISSOCIATION OF NZP ($Ca_{0.5}Sr_{0.5}Zr_4P_6O_{24}$) DURING PLASMA SPRAYING

Rodney W. Trice, Luke N. Brewer and K.T. Faber

Department of Materials Science and Engineering, Robert R. McCormick School of Engineering and Applied Science, Northwestern University, Evanston, IL 60208

(Received July 26, 1999)
(Accepted in revised form December 16, 1999)

Keywords: Plasma spray; TEM; NZP

1. Introduction

Sodium zirconium phosphate ($NaZr_2P_3O_{12}$ or NZP) was first systematically evaluated in the early 1980s by Roy and co–workers (1–2), who demonstrated its extremely low coefficient of thermal expansion (CTE). It was later shown that other group IA and IIA atoms can be ionically substituted into the NZP crystal structure to adjust the CTE (3–5). As a result of their low and tailorable CTEs, NZP's have potential use as a protective coating for silicon–based ceramics (6) and carbon–carbon composites (7).

One technique for the application of ceramic coatings employs plasma–spraying. In this process, powders are injected into a plasma flame, melted, and propelled onto a substrate. The resulting coating microstructure is typically composed of thin lamellae (from each melted particle) stacked on top of one another during each pass of the torch. In the current research, NZP has been plasma–sprayed using the recently patented small particle plasma–spray process (8–10). The microstructure was then analyzed using transmission electron microscopy and x–ray diffraction to identify the phases in the complex coating that resulted.

2. Experimental Methods and Materials

Spray–dried $Ca_{0.5}Sr_{0.5}Zr_4P_6O_{24}$[a] is an NZP compound with ionic substitution of Ca and Sr atoms. This powder, with a mean diameter of 20.8 μm, and the coatings made from it will be referred to simply as NZP in the rest of the paper.

The coating was sprayed to a thickness of $\approx$175 μm using the small–particle plasma–spray (SPPS) process employing non–optimized parameters. An A–3000 Plasma Technik control system with an F4 gun, mounted on a seven–axis ASEA Brown and Boveri IRB 2000 robot, was used to spray the coatings. NZP was fed into the plasma flame using a disc feeder through an externally–mounted SPPS injector. The carrier gas (argon) that fed the powders into the plume was held constant at 5 standard liters per minute (slm). The gun was operated at 35 kW with a plasma gas of Ar (at 40 slm) and H_2 (at 10 slm). The spray distance, measured from the injector to the substrate, was 6 cm. The NZP injector was placed 10 mm from the centerline of the flame. Cooling air was blown on the front and back of the

[a] CS–50, LoTEC Inc., Salt Lake City, UT.

PII: S1359-6462(00)00303-1

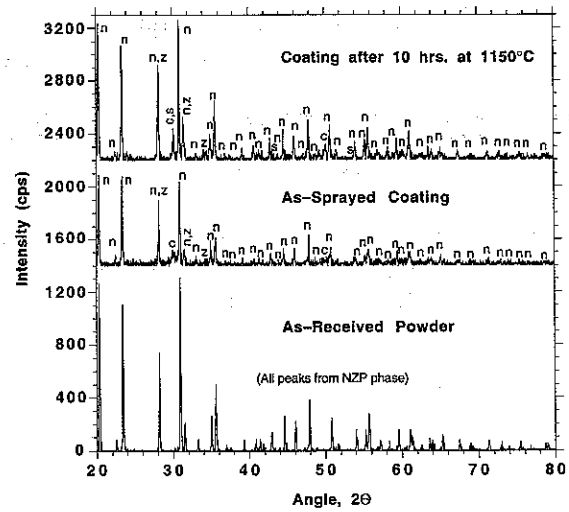

Figure 1. X–ray diffraction patterns from the as–received powder, the as–sprayed coating, and after heat–treatment of the coating (10–hours at 1150°C). (Key: n = NZP, z = *m*–ZrO_2, c = calcium zirconate, s = strontium zirconate).

substrates. The speed of the torch rastering across the substrates was 350 mm/s with a 3 mm drop between passes.

The coating was sprayed on 1018 mild steel substrates that were initially plasma–spray coated with aluminum. The Al layer facilitated removal of the coating as a weak HCl solution preferentially dissolves the aluminum, separating the coating from the substrate. The polished aluminum coating was sand–blasted with 220 grit alumina prior to application of the ceramic coating. The phases present in the starting powder and coatings were determined using X–ray diffraction with Cu–K_α radiation on a Rigaku Geigerflex Diffractometer.

A cross–sectional and planview sample of plasma–sprayed NZP was prepared via the wedge polishing technique[b] and mounted to a copper grid, followed by low–angle argon ion milling[c] to electron transparency. Imaging and electron diffraction were performed in a Hitachi HF2000 cFEG transmission electron microscope (200 keV). It should be noted that all TEM images presented were from the as–sprayed condition. For each TEM sample, three or more thinned areas were investigated. The micrographs presented represent the typical microstructure found in the coating. The local composition of the coating was analyzed in the same instrument using energy dispersive x–ray spectroscopy (EDS).[d] The relative concentrations of Ca, Sr, and Zr were calculated by integrating the K_α peak for each element using DeskTop Spectrum Analyzer (DTSA).[e] In this manner, the Ca–K_α/Zr–K_α and Sr–K_α/Zr–K_α ratios were calculated. Polished cross–sections of the coating also were observed in a Hitachi 3500 VP–SEM in back–scattered imaging mode.

[b]South Bay Technology, San Clemente, CA.
[c]Precision Ion Polishing System, Gatan, Model # 691
[d]Oxford Link QX2000
[e]Developed by the National Institute of Standards and Technology

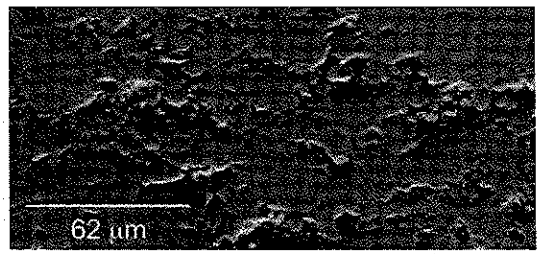

Figure 2. SEM micrograph of a polished cross–section of as–sprayed NZP.

3. Results and Discussion

It has been proposed that a small amount of NZP can dissociate during plasma spraying according to the following reaction (11):

$$Ca_{0.5}Sr_{0.5}Zr_4P_6O_{24} \rightarrow 0.5\ CaZrO_3 + 0.5\ SrZrO_3 + 3\ ZrO_2 + 3\ P_2O_5.$$

The amount of dissociation is a complex function of the spray parameters, with the reaction likely favored for spray conditions that result in a higher–temperature plasma. Towards investigating this hypothesis, x–ray diffraction patterns of the as–received powder and the pulverized coating after plasma spraying are shown in Figure 1. In the as–received powder, all peaks were associated with NZP. However, in the plasma–sprayed coating three distinct phases were observed including NZP, monoclinic zirconia (m–ZrO_2), and a calcium zirconate. The P_2O_5 dissociation product is believed to completely vaporize during processing. The (024) reflection of NZP[f] and the ($\bar{1}11$) reflection of m–ZrO_2[g] overlap at a $2\Theta \approx 28.18°$, resulting in an increase in the magnitude of that peak relative to the maximum peaks of NZP (which occur at a $2\Theta \approx 23.35°$ and $\approx 31.10°$). There are several calcium zirconate phases[h] whose d–spacings correspond to the peaks observed in Figure 1. The calcium

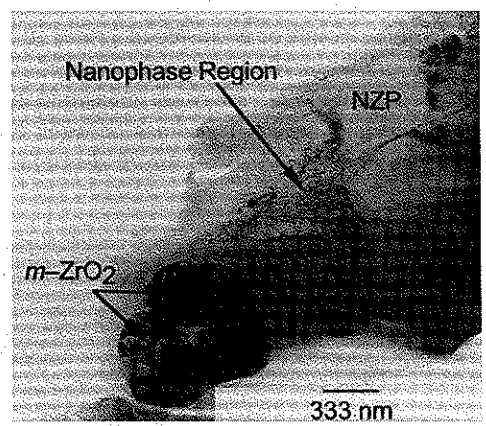

Figure 3. BF TEM micrograph of an as–sprayed NZP coating prepared in cross–section.

[f]JCPDF #33–1312
[g]JCPDF #37–1484
[h]For example, JCPDF #77–2287, #77–2285, #75–359, #26–341, or #24–1074.

TABLE 1
Ratio of Calcium and Strontium to Zirconium in the Phases Indicated as Analyzed by EDS

Phase Location	Ca-K_α/Zr-K_α	Sr-K_α/Zr-K_α
m-ZrO_2 grain in Fig. 3	0	0
NZP grain in Fig. 4	0.02	0.04
Intergranular phase in Fig. 4	0.01	0.01
Nanocrystalline Region in Fig. 5	0.10	0.12

zirconate phases $Ca_xZr_{1-x}O_{2-x}$, with $0.13 \leq x \leq 0.2$, most closely match the experimental results. $SrZrO_3$ was not observed in the as–sprayed coating. However, after a 10–hour heat treatment at 1150°C (see Figure 1) minor peaks of $SrZrO_3$ emerged. These peaks were indexed to JCPDF # 23–561. No diffraction peaks from other phases were observed. From observing the as–sprayed condition presented in Figure 1, it is clear that it is possible to plasma spray NZP and retain it as the majority phase.

The cross–section of a typical region of the as–sprayed coating is shown in Figure 2. These non–optimized coatings were very porous. It is not clear whether the porosity is inter–lamellar or intra–lamellar from the micrograph. However, as described below, little intra–lamellar porosity was observed in the as–sprayed coating using TEM. Besides the large–scale porosity, much of the microstructure was not revealed using SEM, necessitating the use of TEM for microstructural characterization.

A cross–sectional view of a thinned area viewed using TEM is shown in Figure 3. The characteristic plasma–sprayed microstructure consisting of columnar grains and intra–lamellar porosity was not observed in plasma–sprayed NZP. Instead, the coating was comprised of quasi–equiaxed grains, ≈500 nm in diameter, surrounded by much smaller nanocrystalline or amorphous regions. Figure 3 shows both NZP and *m*–ZrO_2 grains, consistent with the x–ray diffraction data for the as–sprayed condition. Close observation of the *m*–ZrO_2 phase reveals its twinned structure and grain sizes ≈400 nm. Monoclinic zirconia was formed during plasma spraying according to the dissociation reaction. As expected, no Ca or Sr was detected in this phase (see Table 1).

Figure 4 is a bright field TEM micrograph of a cluster of grains in a cross–sectional sample. The diffraction pattern from the labeled grain (see Figure 4) was indexed to the NZP phase. The Ca–K_α/Zr–K_α and Sr–K_α/Zr–K_α ratios from this NZP grain, as measured by EDS, were 0.02 and 0.04, respectively. These values are shown in Table 1. The areas between NZP grains were composed of clusters of a crystalline phase, approximately 25 to 50 nm in diameter. Electron diffraction was not

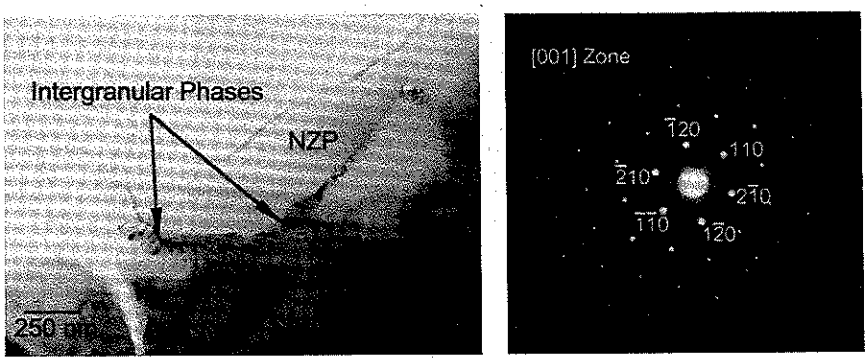

Figure 4. TEM and a diffraction pattern from a typical NZP grain oriented along the [001] zone axis.

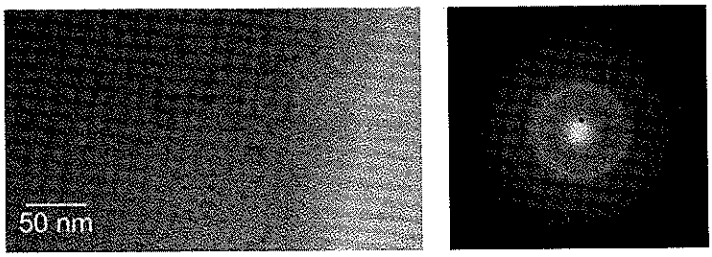

Figure 5. BF TEM image and diffraction pattern of a typical nanocrystalline/amorphous region observed in the plasma–sprayed NZP coating. The rings in the pattern were indexed to a calcium zirconate.

possible from these intergranular phases due to their small size, and therefore, they could not be conclusively identified. However, an analyzed EDS spectrum from this region (see Table 1) indicated similar Ca–K_α/Zr–K_α and Sr–K_α/Zr–K_α ratios to that of the NZP phase.

A close–up of a nanocrystalline/amorphous region for a sample prepared in planview is shown in Figure 5. Small crystallites ≈6 nm in diameter are evident in the TEM micrograph. As shown in Table 1, elemental spectra revealed the region to be rich in calcium and strontium, with Ca–K_α/Zr–K_α and Sr–K_α/Zr–K_α ratios of 0.10 and 0.12, respectively. These ratios are considerably higher than observed in the NZP grain analyzed above. The accompanying diffraction pattern resulting from the nanocrystalline regions was indexed to calcium zirconate, consistent with the high concentration of Ca. While the strontium concentration was also rich, no crystalline phases from $SrZrO_3$ were observed in the diffraction pattern indicated in Figure 5, indicating that Sr was primarily located in the amorphous regions. This was consistent with the x–ray diffraction results of the as–sprayed coating which revealed no crystalline $SrZrO_3$ phase.

4. Conclusions

The microstructure and phase composition of plasma–sprayed NZP was investigated using standard x–ray diffraction and TEM techniques. The coating was composed primarily of clusters of sub–micron grains of NZP surrounded by amorphous or nanocrystalline regions. The typical columnar grain morphology and intra–lamellar porosity observed in most plasma–sprayed coatings was not observed in the current coating. Small fractions of monoclinic zirconia and calcium zirconate, attributed to dissociation of the NZP during plasma–spraying, were observed in the as–sprayed coating via x–ray diffraction and TEM. While amorphous regions rich in strontium were observed, the $SrZrO_3$ phase expected from the dissociated reaction did not appear until after a 10–hour heat treatment at 1150°C.

This research reveals that NZP can be plasma–sprayed as the majority phase, but that the microstructure is not what one would expect from existing plasma–spray literature. The complexity of the as–sprayed coating, including nanocrystalline and amorphous regions, indicates a non–equilibrium microstructure. In light of this, it will be necessary to analyze the evolution of this microstructure at high temperatures.

Acknowledgments

The authors gratefully acknowledge the financial support of the U.S. Department of Energy, Federal Energy Technology Center, Cooperative Agreement No. DE–FC21-92MC29061, subcontract 96-01–SR047, the National Science Foundation, contract No. DMR–9974013, and the Department of Defense

NDSEG Fellowship. The authors also wish to thank Rick Marzec for assistance during plasma–spraying and Tom Easley for helpful comments while preparing the manuscript.

References

1. J. Alamo and R. Roy, J. Am. Ceram. Soc. 67, C-78 (1984).
2. R. Roy, D. K. Agrawal, J. Alamo, and R. A. Roy, Mater. Res. Bull. 19, 471 (1984).
3. S. Y. Limaye, D. K. Agrawal, R. Roy, and Y. Mehrotra, J. Mater. Sci. 26, 93 (1991).
4. V. Srikanth, E. C. Subbarao, D. K. Agrawal, C.-Y. Huang, R. Roy, and G. V. Rao, J. Am. Ceram. Soc. 74, 365 (1991).
5. R. Brochu, M. El-Yacoubi, M. Louer, A. Serghini, M. Alami, and D. Louer, Mater. Res. Bull. 32, 15 (1997).
6. W. Y. Lee, K. M. Cooley, C. C. Berndt, D. L. Joslin, and D. P. Stinton, J. Am. Ceram. Soc. 79, 2759 (1996).
7. D. K. Agrawal, G. Harshe, E. Breval, and R. Roy, J. Mater. Res. 11, 3158 (1996).
8. R. W. Trice, Y. J. Su, K. T. Faber, Hsin Wang, and W. Porter, Mater. Sci. Eng. A. A272, 284 (1999).
9. R. W. Trice and K. T. Faber, J. Am. Ceram. Soc. in press.
10. T. F. Bernecki and D. R. Marron, U.S. Patent #5,744,777 (1998) and #5,858,470 (1999).
11. Private communication, Rama Nageswaran at LoTEC Industries.